Modulated and unmodulated structures, and the transport mechanisms in the triangular lattice system Na_xCoO_2 with $x \simeq$ 0.48, 0.58 and 0.65

2007 J. Phys.: Condens. Matter 19 186213

(http://iopscience.iop.org/0953-8984/19/18/186213)

IOP PUBLISHING JOURNAL OF PHYSICS: CONDENSED MATTER

J. Phys.: Condens. Matter **19** (2007) 186213 (14pp) doi:10.1088/0953-8984/19/18/186213

Modulated and unmodulated structures, and the transport mechanisms in the triangular lattice system Na_xCoO_2 with $x \simeq 0.48$, 0.58 and 0.65

Masashige Onoda and Tomohiro Ikeda

Institute of Physics, University of Tsukuba, Tennodai, Tsukuba 305-8571, Japan

E-mail: onoda@sakura.cc.tsukuba.ac.jp

Received 23 January 2007, in final form 4 March 2007
Published 11 April 2007
Online at stacks.iop.org/JPhysCM/19/186213

Abstract

The crystal structures of the triangular lattice system γ-phase Na_xCoO_2 with compositions of $x \simeq 0.48$, 0.58 and 0.65 have been determined by means of x-ray four-circle diffraction. $Na_{0.58}CoO_2$ has lattice constants of $a_h = 2.8180(5)$ and $c_h = 11.005(9)$ Å with space group $P6_3/mmc$ and does not exhibit structural modulation. On the other hand, $Na_{0.65}CoO_2$ has a $P6_3/mmc$-type superlattice with a doubled unit cell of $a_{sh} = 5.6527(5)$ and $c_{sh} = 10.9356(10)$ Å, and $Na_{0.48}CoO_2$ indicates a $Pmmn$-type superlattice with $a_{so} = 5.6261(5)$, $b_{so} = 11.1406(10)$ and $c_{so} = 4.8723(5)$ Å. The structural modulation for $x \simeq 0.65$ is attributed to the incomplete order of Na ions without an order for Co valence, while that for $x \simeq 0.48$ results in almost complete Na order and partial valence order for Co. For $x \simeq 0.48$, the metal–poor metal transition occurs at about 50 K. The electrical resistivities for $x \simeq 0.58$ and 0.65 follow a $T^{3/2}$ dependence below 200 and 80 K, respectively, which may be due to antiferromagnetic spin fluctuations in three dimensions. At higher temperatures, the resistivities for the CoO_2 plane have a T^1 dependence, likely due to an enhancement of two dimensionality. For $x \simeq 0.65$, the resistivity maximum appears at about 250 K, which may be attributed to the renormalization effect of the Fermi surface by the fluctuations.

M Supplementary data are available from stacks.iop.org/JPhysCM/19/186213

1. Introduction

The transition-metal oxide system has been investigated from various viewpoints to clarify the basic properties of correlated electron, electron–phonon coupling and quantum spin fluctuation systems, and to search for novel phenomena and functions. The final goal for this research is to understand quantitatively a relation between the crystal structures and the physical properties.

Triangular lattice systems have attracted considerable attention, since the proposal of resonating-valence-bond theory regarding a spin–liquid ground state for Heisenberg-type interaction [1, 2]. The spatially isotropic interactions lead to long-range magnetic order [3], but, in some cases, to characteristic ground states such as spin–trimer [4] and spin–ice [5]. The recent discovery of superconductivity for the hydrated triangular lattice system $Na_{0.3}CoO_2{\cdot}1.3H_2O$ [6] as well as the reporting of an enhanced thermoelectric power factor for the parent metallic compound Na_xCoO_2 [7] throws up more interest in the triangular lattice system.

The Na_xCoO_2 system has several different phases with sheets of edge-sharing CoO_6 octahedra interleaved by Na [8]. The stacking sequence of the oxygen layers leads to a number of sheets for a unit cell. The so-called γ phase at which this work is aimed has a two-layer structure. Using neutron powder diffraction, the structure of this phase was modelled for $Na_{0.74}CoO_2$ [9] and then a refinement for $Na_{0.61}CoO_2$ was also reported [10]. This structure with space group $P6_3/mmc$ is basically described in terms of CoO_6 octahedra which are joined by sharing edges to form a two-dimensional triangular lattice of Co ions. Between these lattices, the Na atoms labelled Na1 and Na2 with trigonal prismatic environments reside in some occupation probability. In this system, there exist various structural modulations [11]. $Na_{0.5}CoO_2$ may have an Na ordered structure forming one-dimensional zigzag chains [12].

The phase diagram of Na_xCoO_2 as a function of the Na concentration [13] indicates that, as x increases, the ground state goes from a charge-ordered insulator at $x = \frac{1}{2}$ [12, 14] to a Curie–Weiss metal around $x \approx 0.7$, and then to a spin density wave (SDW) state for higher x [15, 16]. The structural and electronic properties of Na_xCoO_2 with nominal compositions of $0.8 \leqslant x \leqslant 1$ annealed at temperatures from 923 to 1123 K vary significantly with annealing temperature, since the chemical composition as well as the local structure is modified [17]. Most of the investigations performed to date are for the specimens annealed above the critical temperature T_{ac}, which ranges from 973 to 1023 K. In order to clarify the properties of Na_xCoO_2 completely, it is very necessary to know the absolute chemical composition. In addition, the first-order phase transitions of the electrical resistivities are observed irrespective of the cooling condition likely due to the ordering of Na ions. The irreversible transitions in the heating process also appear with fast cooling to a certain temperature.

As will be discussed later, the electrical transitions described above do not exist for the present single-crystal specimens with $0.48 \leqslant x \leqslant 0.65$, outside of the composition for the polycrystalline specimens. This work describes the crystal structures and the transport mechanisms for these single-crystal specimens. The modulated superlattice structures and the unmodulated superlattice structures determined precisely from x-ray four-circle diffraction are presented in section 2, and the transport mechanisms revealed through measurements of electrical resistivity, thermoelectric power and magnetic susceptibility are described in section 3. Section 4 is devoted to conclusions.

2. Crystal structures

2.1. Crystal growth

Single-crystal specimens of Na_xCoO_2 with $x \simeq 0.58$ and 0.65 were prepared by the flux method. Mixtures with a Na_2CO_3:Co_3O_4:NaCl ratio of 1:1:7 were put in an electric furnace. The temperature was increased to 1323 K for 3 h, held constant for 12 h and cooled to 1123 K for 80 h, and then cooled to room temperature for 8 h. The $Na_{0.48}CoO_2$ single crystal was prepared by mixing 10^{-3} kg of $Na_{0.65}CoO_2$ with 6.6 M of Br_2 dissolved in acetonitrile through 5 days of stirring. The chemical compositions presented here were determined from

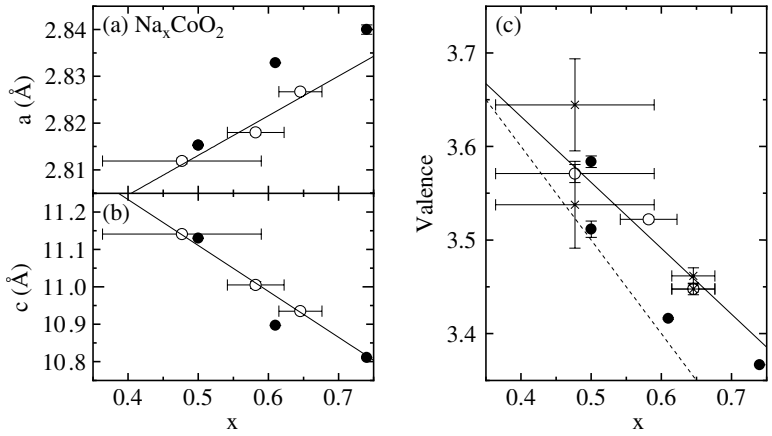

Figure 1. (a), (b) The hexagonal lattice constants for the unmodulated cell and the average cells, and (c) the Co valences of Na_xCoO_2 as a function of the Na concentration listed in table 2. Here, the data for $x = 0.5$, 0.61 and 0.74 in (a), (b) indicated by the full circles are taken from [12, 10, 9], respectively, and those in (c) are calculated on the basis of their atomic parameters. The full lines in (a)–(c) show least-squares fits for the present data and the dotted line in (c) indicates the valence calculated from the chemical composition. The crosses in (c) denote results for the superlattice structures with $x \simeq 0.48$ and 0.65.

analysis for the unmodulated structure and the average structures described below. The Na:Co ratio for $Na_{0.65}CoO_2$ agreed well with the result obtained from inductively coupled plasma-optical emission spectroscopy at room temperature using a Nippon Jarrell-Ash ICAP-575 spectrometer.

2.2. X-ray four-circle diffraction measurements

The x-ray four-circle diffraction measurements were performed on a Nonius CAD4 and a Rigaku AFC-7R (custom made) with graphite-monochromated Mo Kα radiation at 297 K. For the unmodulated cell and the average cells of Na_xCoO_2, the crystal data are obtained as listed in table 1 from the systematic absences of reflections, a statistical analysis of the intensity distribution, and the successful solution and refinement of the structure. The composition dependences of the hexagonal lattice constants a_h and c_h are plotted in figures 1(a) and (b), respectively.

In order to confirm possible superlattice reflections, grid-scan measurements were performed on the basis of the above cells for all of the crystals. The patterns for $l = 0$ and 2 are shown in figure 2, where the radia of the spots are scaled logarithmically after the subtraction of the constant background. The strong ring around the origin is meaningless. $Na_{0.58}CoO_2$ has few distinct superlattice reflections and may be regarded as being unmodulated. On the other hand, $Na_{0.65}CoO_2$ has clear spots at positions with a doubled unit cell for a_h and b_h. For $Na_{0.48}CoO_2$, complicated spot patterns appear due to the presence of twinning of crystals, as will be described later. These additional spots are not diffusive.

Intensity data for the structure analyses were collected using the $\omega-2\theta$ scan technique, and corrections for Lorentz polarization and absorption effects were applied. All of the structures were determined by direct methods [18], expanded using Fourier techniques, and refined by means of full-matrix least-squares calculations [18, 19]. Here, atomic scattering factors were taken from [20] and anomalous dispersion effects were included, with the values given by [21].

Table 1. The crystal data and a summary of the intensity measurements and refinements of Na_xCoO_2.

	$Na_{0.65}CoO_2$		$Na_{0.58}CoO_2$	$Na_{0.48}CoO_2$	
	Average (h)	Superlattice (sh)	No modulation (h)	Average (h)	Superlattice (so)
Space group	$P6_3/mmc$	$P6_3/mmc$	$P6_3/mmc$	$P6_3/mmc$	$Pmmn$
$a_{h,sh,so}$ (Å)	2.8267(3)	5.6527(5)	2.8180(5)	2.8119(6)	5.6261(5)
b_{so} (Å)	—	—	—	—	11.1406(10)
$c_{h,sh,so}$ (Å)	10.9351(10)	10.9356(10)	11.005(9)	11.1410(10)	4.8723(5)
$V_{h,sh,so}$ (Å^3)	75.668(13)	302.61(5)	75.69(6)	76.29(2)	305.39(5)
$2\theta_{max}$	99.2	79.9	99.4	89.7	89.7
R_{int}	0.031	0.044	0.081	0.0346	—
Translation factor	0.34–0.89	0.28–0.89	0.32–0.90	0.15–0.59	0.10–0.57
No. of reflections	189	400	188	156	852
No. of variables	14	28	13	14	30
$R1$[a]	0.0232	0.0381	0.0293	0.0600	0.0640

[a] $R1 = (\sum ||F_o|-|F_c||)/(\sum |F_o|)$, with $|F_o|$ and $|F_c|$ being the observed and calculated structure factors, respectively.

Tables of the observed and calculated structure factors are provided in supplementary data files (available at stacks.iop.org/JPhysCM/19/186213).

2.3. Unmodulated structure of $Na_{0.58}CoO_2$ and average structures of $Na_{0.48}CoO_2$ and $Na_{0.65}CoO_2$

Since $Na_{0.58}CoO_2$ does not show significant superlattice reflection, the precise atomic parameters for the unmodulated structure of Na_xCoO_2 are obtained. For a comparison, the average structures for $x \simeq 0.48$ and 0.65 that reflect possible displacement and/or intensity modulations through a Fourier transform of the main reflections are determined by neglecting the superlattice reflections. The atomic coordinates, equivalent isotropic thermal parameters, and anisotropic displacement parameters for all of the compositions are listed in table 2. Here, all of the parameters are refined *without any non-obvious constraint* in contrast to the previous analyses based on the powder profiles, where it is assumed that the thermal parameters of Na1 and Na2 are the same [9] or that the Na2 site is split virtually [10]. Selected interatomic distances are listed in table 3. The clinographic view of the crystal structure of $Na_{0.58}CoO_2$ and the projection on the ab-plane are shown in figures 3(a) and (b), respectively.

As introduced in section 1, there exists a two-dimensional triangular lattice of Co ions linked by edge-shared CoO_6 octahedra. Between these lattices, the Na1 and Na2 sites, corresponding to those of 2b and 2c for the space group $P6_3/mmc$ respectively, are partially occupied with trigonal prismatic environments. Since the Na1–Na2 distance is significantly smaller than that expected from the ionic radius of octahedrally coordinated Na^+ (1.02 Å [22]), these sites cannot be occupied simultaneously due to the strong Coulomb repulsion. The Co–Na1 distance along the hexagonal c-direction is smaller than the Co–Co distance, which may also cause an influence on the electronic properties. For $x \simeq 0.58$ and 0.65, the occupancy for Na1 is smaller than that for Na2, while for $x \simeq 0.48$ their ratio is compatible. With decreasing x, the occupancy for Na1 increases and that for Na2 decreases.

The Co–O distance listed in table 3 varies from 1.9050(10) to 1.892(3) Å as x decreases. By using the bond length versus bond strength relation [23], the effective valences at the Co site are estimated as listed in this table and their composition dependence is shown in figure 1(c). These values are roughly consistent with those calculated from the chemical formula $4 - x$, as

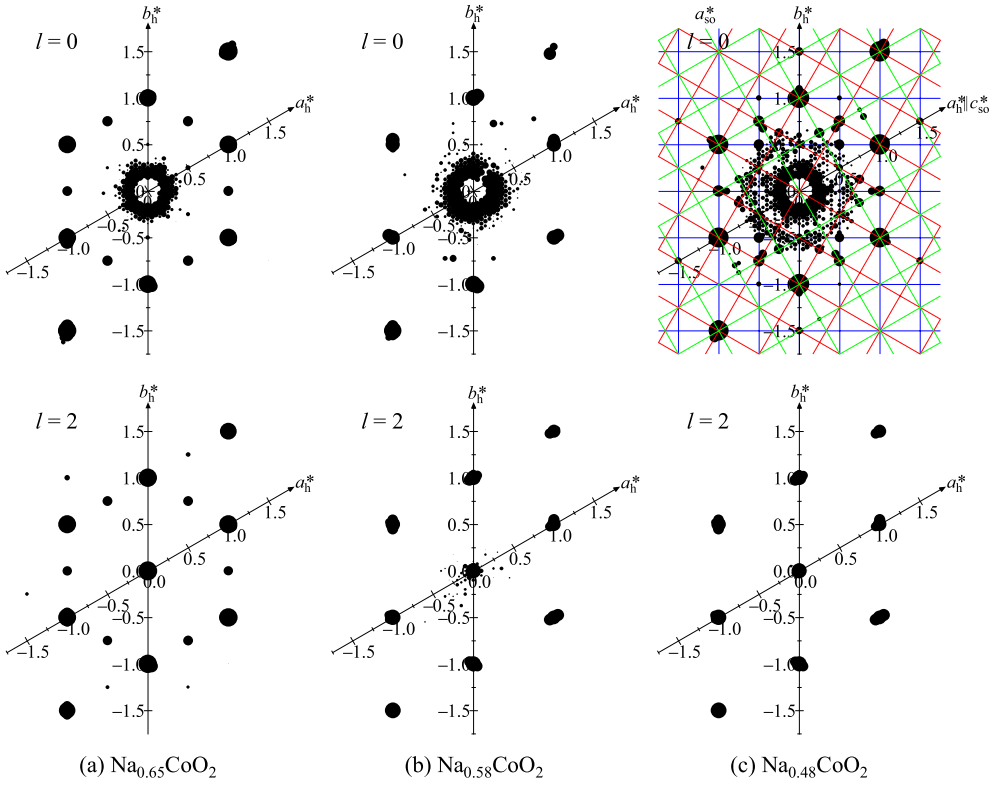

Figure 2. The grid-scan patterns on the basis of the unmodulated hexagonal cell and the averaged cells of Na_xCoO_2 with (a) $x \simeq 0.65$, (b) 0.58 and (c) 0.48 at 297 K, where the radia of the spots are scaled logarithmically after the subtraction of constant background. The upper and lower panels indicate the data for $l = 0$ and 2, respectively. In the upper panel of (c), the twinned cells with the orthorhombic symmetry are expressed by three kinds of colour grids.

(This figure is in colour only in the electronic version)

drawn by the dotted line, suggesting that both Co and O atoms are occupied fully. The Na1–O and Na2–O distances range from 2.3937(14) to 2.434(4) Å, which indicates that the ionic radii of Na is 1.01–1.05 Å. This is consistent with the value for six-coordinated Na ion.

2.4. Modulated structures of $Na_{0.65}CoO_2$ and $Na_{0.48}CoO_2$

2.4.1. $Na_{0.65}CoO_2$. $Na_{0.65}CoO_2$ has a doubled unit cell for a_h and b_h. Detailed intensity measurements with the condition of triclinic symmetry indicate that this superlattice cell is hexagonal, as in the case of the average cell; that is, the lattice constants are given by $a_{sh} \simeq 2a_h$ and $c_{sh} \simeq c_h$. The ratio of the number of superlattice reflections to that of the total reflections with $|F_o| \geqslant 3\sigma(|F_o|)$, $\sigma(|F_o|)$ being a standard deviation of the observed structure factor, is 0.25. The atomic coordinates, the anisotropic displacement parameters and the selected interatomic distances for the hexagonal superlattice are listed in tables 4–6, respectively. Figures 4(a) and (b) show the clinographic view of the crystal structure and the projection on the *ab*-plane, respectively. The Co ions labelled Co1 and Co2 are located at the crystallographically independent 2a and 6g sites for the space group $P6_3/mmc$, respectively, and they are surrounded octahedrally by O ions. The O ions also have two sites of 4f and

Table 2. Atomic coordinates, equivalent isotropic thermal parameters B_{eq} (Å^2), and anisotropic displacement parameters U_{ij} for the unmodulated structure of $Na_{0.58}CoO_2$ and the average structures of $Na_{0.65}CoO_2$ and $Na_{0.48}CoO_2$ at 297 K, where $B_{eq} = \frac{8}{3}\pi^2[U_{11}(aa^*)^2 + U_{22}(bb^*)^2 + U_{33}(cc^*)^2 + 2U_{12}aa^*bb^*\cos\gamma + 2U_{13}aa^*cc^*\cos\beta + 2U_{23}bb^*cc^*\cos\alpha]$, U_{ij} being defined in the thermal factor form $T = \exp[-2\pi^2(a^{*2}U_{11}h^2 + b^{*2}U_{22}k^2 + c^{*2}U_{33}l^2 + 2a^*b^*U_{12}hk + 2a^*c^*U_{13}hl + 2b^*c^*U_{23}kl)]$. The sites for 2a, 2b, 2c and 4f correspond to (0 0 0), (0 0 $\frac{1}{4}$), ($\frac{1}{3}$ $\frac{2}{3}$ $\frac{1}{4}$) and ($\frac{2}{3}$ $\frac{1}{3}$ z), respectively. For all atoms, $U_{11} = U_{22}$, $U_{12} = U_{11}/2$ and $U_{13} = U_{23} = 0$.

Atom	Site	Parameter	$Na_{0.65}CoO_2$ Average	$Na_{0.58}CoO_2$ No modulation	$Na_{0.48}CoO_2$ Average
Co	2a	B_{eq}	0.389(7)	0.360(8)	0.50(3)
		U_{11}	0.003 37(11)	0.002 77(12)	0.0042(4)
		U_{33}	0.008 02(13)	0.008 13(14)	0.0105(5)
Na1	2b	B_{eq}	1.3(2)	1.9(2)	2.5(10)
		U_{11}	0.017(3)	0.030(4)	0.038(18)
		U_{33}	0.015(3)	0.011(3)	0.019(14)
		Occupancy	0.20(2)	0.24(2)	0.26(6)
Na2	2c	B_{eq}	3.7(2)	2.9(3)	4.1(18)
		U_{11}	0.066(4)	0.050(5)	0.07(3)
		U_{33}	0.0082(15)	0.009(2)	0.007(11)
		Occupancy	0.45(2)	0.34(2)	0.22(5)
O	4f	z	0.089 87(18)	0.088 65(17)	0.0872(5)
		B_{eq}	0.565(17)	0.481(19)	0.48(6)
		U_{11}	0.0055(2)	0.0043(3)	0.0033(9)
		U_{33}	0.0104(4)	0.0096(4)	0.0118(16)

Table 3. Interatomic distances (Å) and Co valences for the unmodulated structure of $Na_{0.58}CoO_2$ and the average structures of $Na_{0.65}CoO_2$ and $Na_{0.48}CoO_2$ at 297 K, where the symmetry operations are: (a) $x,\ y,\ z$; (b) $-1+x,\ -1+y,\ z$; (c) $-1+x,\ y,\ z$; (d) $-x,\ -y,\ -z$; (e) $1-x,\ -y,\ -z$; (f) $1-x,\ 1-y,\ -z$; (g) $-x+y,\ -x,\ \frac{1}{2}-z$; (h) $-x+y,\ 1-x,\ \frac{1}{2}-z$; (i) $1-x+y,\ 1-x,\ \frac{1}{2}-z$; (j) $x,\ 1+y,\ z$; (k) $1-x+y,\ 2-x,\ \frac{1}{2}-z$; (l) $x-y,\ x,\ -\frac{1}{2}+z$; (m) $x,\ -1+y,\ z$; (n) $x-y,\ -1+x,\ -\frac{1}{2}+z$; (o) $1+x-y,\ x,\ -\frac{1}{2}+z$; (p) $1+x,\ y,\ z$; and (q) $-1+x,\ -2+y,\ z$.

	$Na_{0.65}CoO_2$ Average	$Na_{0.58}CoO_2$ No modulation	$Na_{0.48}CoO_2$ Average
Co^a–$O^{a,b,c,d,e,f}$	1.9050(10)	1.8971(9)	1.892(3)
Co valence	3.448(3)	3.522(3)	3.571(10)
$Na1^a$–$O^{a,b,c,g,h,i}$	2.3937(14)	2.4084(13)	2.434(4)
$Na2^a$–$O^{a,c,j,h,i,k}$	2.3937(14)	2.4084(13)	2.434(4)
Co^a–$Na1^{a,l}$	2.7338	2.7513	2.7853
Co^a–$Na2^{a,b,l,m,n,o}$	3.1839	3.1964	3.2239
$Na1^a$–$Na2^{a,b,m}$	1.6320	1.6270	1.6235
$Na1^a$–$Na2^{c,p,q}$	3.2640	3.2540	3.2469

12k labelled O1 and O2. The Na1 and Na2 ions reside at 6h sites with occupancy factors of 0.31(2) and 0.43(2), respectively, and they have trigonal prismatic environments. The Na concentration obtained here is slightly larger than that for the average structure, but it is within a standard deviation. The most important difference between this superlattice structure and the unmodulated structure is that the Na ion does not exist right above the Co1 ion. In addition, the Na ion does not exist around the position ($\frac{2}{3}$ $\frac{1}{3}$ $\frac{1}{4}$) expected on the basis of the unmodulated structure. There remains an anomalously short Na1–Na2 pair of 1.704(7) Å for which simultaneous occupation is inhibited, but other Na–Na pairs have distances longer than

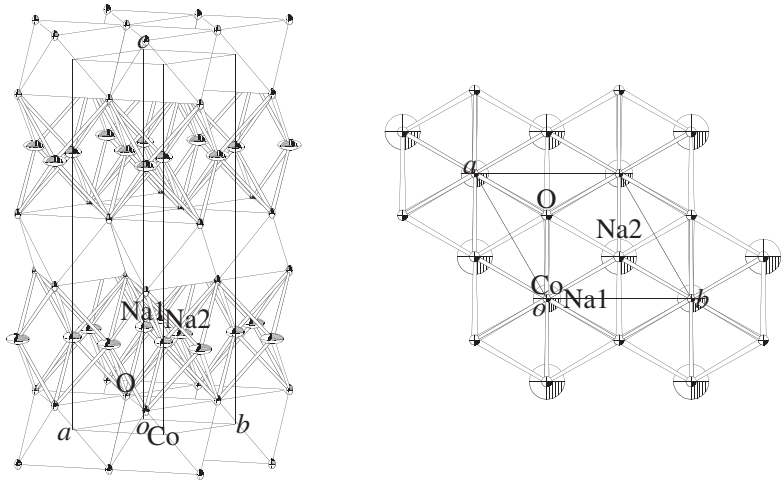

(a) (b)

Figure 3. The crystal structures of $Na_{0.58}CoO_2$ at 297 K: (a) the clinographic view with octahedra for Co and (b) the projection on the *ab*-plane, where the ellipsoids are drawn at the 50% probability level.

Table 4. Atomic coordinates and equivalent isotropic thermal parameters B_{eq} (Å^2) of $Na_{0.65}CoO_2$ at 297 K.

Atom	Site	Occupancy	x	y	z	B_{eq}
Co1	2a	1	0	0	0	0.41(3)
Co2	6g	1	$\frac{1}{2}$	0	0	0.415(19)
Na1	6h	0.31(2)	0.4980(13)	0.5020(13)	$\frac{1}{4}$	2.8(3)
Na2	6h	0.43(2)	0.1513(9)	0.3025(19)	$\frac{1}{4}$	3.8(3)
O1	4f	1	$\frac{1}{3}$	$\frac{2}{3}$	0.0923(7)	0.62(11)
O2	12k	1	0.3347(8)	0.1673(4)	0.0888(3)	0.58(4)

Table 5. Anisotropic displacement parameters U_{ij} of $Na_{0.65}CoO_2$ at 297 K.

Atom	U_{11}	U_{22}	U_{33}	U_{12}	U_{13}	U_{23}
Co1	0.0044(5)	0.0044(5)	0.0068(7)	0.0022(2)	0	0
Co2	0.0035(3)	0.0029(5)	0.0092(3)	0.0014(2)	0.0002(2)	0.0003(4)
Na1	0.019(4)	0.019(4)	0.032(6)	−0.015(5)	0	0
Na2	0.093(7)	0.021(4)	0.007(2)	0.010(2)	0	0
O1	0.006(2)	0.006(2)	0.012(2)	0.0028(10)	0	0
O2	0.007(2)	0.0049(11)	0.0111(11)	0.0033(10)	−0.0008(14)	−0.0004(7)

2.565(8) Å. For all atoms, the anisotropic displacement parameters in table 5 are within a normal range.

The effective valences at the Co1 and Co2 sites are estimated to be 3.448(6) and 3.462(9), respectively, as indicated in table 6 and figure 1(c). These values are almost the same as each other and agree with the result for the average structure (table 3). The Na1–O and Na2–O distances range from 2.361(8) to 2.480(8) Å, corresponding to the value for six-coordinated Na ions [22].

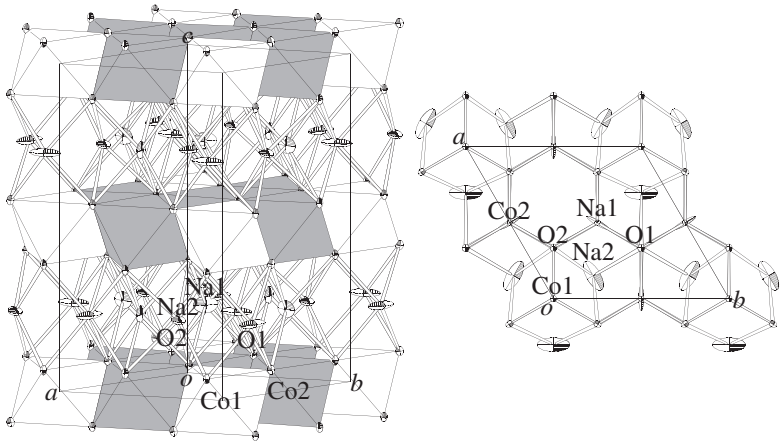

(a) (b)

Figure 4. The crystal structures of $Na_{0.65}CoO_2$ at 297 K with the ellipsoids drawn at the 50% probability level: (a) the clinographic view with the white and shaded octahedra for Co1 and Co2, respectively, and (b) the projection on the *ab*-plane.

Table 6. Interatomic distances (Å) and Co valences for the superlattice structure of $Na_{0.65}CoO_2$ at 297 K, where the symmetry operations are: $(a)\ x,\ y,\ z$; $(b)\ -y,\ x-y,\ z$; $(c)\ -x+y,\ -x,\ z$; $(d)\ -x,\ -y,\ -z$; $(e)\ y,\ -x+y,\ -z$; $(f)\ x-y,\ x,\ -z$; $(g)\ x,\ -1+y,\ z$; $(h)\ 1-x,\ 1-y,\ -z$; $(i)\ 1-y,\ x-y,\ z$; $(j)\ 1-x,\ -y,\ -z$; $(k)\ -x+y,\ 1-x,\ \frac{1}{2}-z$; $(l)\ 1-x+y,\ 1-x,\ z$; $(m)\ 1-x+y,\ 1-x,\ \frac{1}{2}-z$; $(n)\ x,\ y,\ \frac{1}{2}-z$; $(o)\ -y,\ x-y,\ \frac{1}{2}-z$; $(p)\ x-y,\ x,\ -\frac{1}{2}+z$; $(q)\ -x,\ -y,\ -\frac{1}{2}+z$; $(r)\ y,\ -x+y,\ -\frac{1}{2}+z$; $(s)\ 1+x-y,\ x,\ -\frac{1}{2}+z$; $(t)\ 1-y,\ 1+x-y,\ z$; and $(u)\ -x+y,\ 1-x,\ z$.

Metal–O		Metal–metal	
$Co1^a$–$O2^{a,b,c,d,e,f}$	1.905(2)	$Co1^a$–$Na2^{a,b,c,p,q,r}$	3.109(2)
Co1 valence	3.448(6)	$Co2^a$–$Na1^{i,r}$	2.733 97(5)
$Co2^a$–$O1^{g,h}$	1.919(4)	$Co2^a$–$Na2^{c,i,r,s}$	3.226(2)
$Co2^a$–$O2^{a,e,i,j}$	1.896(4)	$Na1^a$–$Na1^{i,l}$	2.860(11)
Co2 valence	3.462(9)	$Na1^a$–$Na1^{t,u}$	2.792(11)
$Na1^a$–$O1^{a,k}$	2.361(8)	$Na1^a$–$Na2^{a,t}$	1.704(7)
$Na1^a$–$O2^{a,l,m,n}$	2.406(5)	$Na1^a$–$Na2^{c,l}$	3.200(7)
$Na2^a$–$O1^{a,k}$	2.480(8)	$Na1^a$–$Na2^{u}$	3.395(13)
$Na2^a$–$O2^{a,b,n,o}$	2.357(5)	$Na2^a$–$Na2^{b,c}$	2.565(8)
		$Na2^a$–$Na2^{t,u}$	3.088(8)

2.4.2. $Na_{0.48}CoO_2$. The grid-scan patterns of $Na_{0.48}CoO_2$ shown in figure 2(c) indicate that the present crystal is twinned with the orthorhombic cell of $a_{so} \simeq 2a_h$, $b_{so} \simeq c_h$ and $c_{so} \simeq \sqrt{3}a_h$, related by the matrix

$$\begin{pmatrix} \boldsymbol{a} \\ \boldsymbol{b} \\ \boldsymbol{c} \end{pmatrix}_{so} = \begin{pmatrix} 0 & 2 & 0 \\ 0 & 0 & 1 \\ 2 & 1 & 0 \end{pmatrix} \begin{pmatrix} \boldsymbol{a} \\ \boldsymbol{b} \\ \boldsymbol{c} \end{pmatrix}_{h}. \tag{1}$$

Here, this supercell is the same as that evaluated previously for $Na_{0.5}CoO_2$ [13, 12]. Two twin matrices for the reciprocal space are given by

$$\boldsymbol{T}_1 = \begin{pmatrix} -\frac{1}{2} & 0 & 1 \\ 0 & -1 & 0 \\ \frac{3}{4} & 0 & \frac{1}{2} \end{pmatrix}, \tag{2}$$

Table 7. Atomic coordinates, isotropic thermal parameters B (Å^2) for Na and O and the equivalent ones B_{eq} (Å^2) for Co of $Na_{0.48}CoO_2$ at 297 K.

Atom	Site	Occupancy	x	y	z	B, B_{eq}
Co1	4e	1	$\frac{1}{4}$	0.003 54(13)	0.0023(3)	0.58(3)
Co2	4d	1	0	0	$\frac{1}{2}$	0.67(4)
Na1	2b	1	$\frac{1}{4}$	$-\frac{1}{4}$	0.971(2)	2.00(19)
Na2	2a	1	$\frac{1}{4}$	$\frac{1}{4}$	0.644(2)	2.03(19)
O1	4e	1	$\frac{1}{4}$	0.0874(6)	0.333(5)	0.96(10)
O2	4e	1	$\frac{1}{4}$	−0.0840(6)	0.675(4)	0.81(11)
O3	8g	1	0.0018(9)	−0.0881(5)	0.165(5)	1.09(7)

Table 8. Anisotropic displacement parameters U_{ij} of $Na_{0.48}CoO_2$ at 297 K.

Atom	U_{11}	U_{22}	U_{33}	U_{12}	U_{13}	U_{23}
Co1	0.0070(15)	0.0110(6)	0.0040(19)	0	0	−0.0008(8)
Co2	0.0066(16)	0.0121(7)	0.007(2)	−0.0008(3)	−0.0011(6)	0.0004(8)

$$\boldsymbol{T}_2 = \begin{pmatrix} \frac{1}{2} & 0 & 1 \\ 0 & -1 & 0 \\ \frac{3}{4} & 0 & -\frac{1}{2} \end{pmatrix}. \tag{3}$$

Following the above model, the intensity data are transformed through the ROTAX procedure [24] in the WinGX program [25]. Here, partially overlapped reflections with significantly asymmetric backgrounds were removed in the criterion of $I_b^{max}/I_b^{min} = 2$, with $I_b^{max(min)}$ being the maximum (minimum) counts for the background, respectively. The ratio of the number of superlattice reflections to that of the total with $|F_o| \geqslant 3\sigma(|F_o|)$ is 0.43.

The atomic coordinates, the anisotropic displacement parameters and the selected interatomic distances for the orthorhombic superlattice (table 1) are listed in tables 7–9, respectively[1]. Here, owing to the significant twinning, the thermal parameters for Na and O ions are refined isotropically and the occupancies of Na are fixed at unity, which satisfies the result for the average structure within a standard deviation. Since non-obvious constraints for the structural parameters, where some atom positions are fixed and the isotropic thermal parameters for like atoms are the same [12], are *not* applied to this refinement, the atomic parameters presented here are more reliable. The clinographic view of the crystal structure and the projection on the ac-plane are indicated in figures 5(a) and (b), respectively. The octahedrally coordinated Co ions labelled Co1 and Co2 reside in the crystallographically independent 4e and 4d sites for the space group $Pmmn$, respectively. The O ions have three sites 4e, 4e and 8g, labelled O1, O2 and O3, respectively. The Na1 and Na2 ions having trigonal prismatic environments are located at 2b and 2a sites with full occupancy. The $Na1O_6$ prism shares faces with CoO_6 octahedra and the Na2 prism shares edges. In this structure, the Na atom does not reside right above the Co2 ion and the unstable Na–Na pair does not exist, since the shortest distance for the pair is 3.380(7) Å, as listed in table 9.

The Co–O distances for the $Co1O_6$ octahedra range from 1.86(2) to 1.903(11) Å, while those for the $Co2O_6$ are almost identical (1.90 Å). The bond length versus bond strength relation provides effective valences of 3.64(4) for Co1 and 3.54(4) for Co2 (figure 1(c)). These are slightly different to each other and their mean value is consistent with the result for the

[1] This work uses the standard setting of the space group $Pmmn$ for the description of crystal structure.

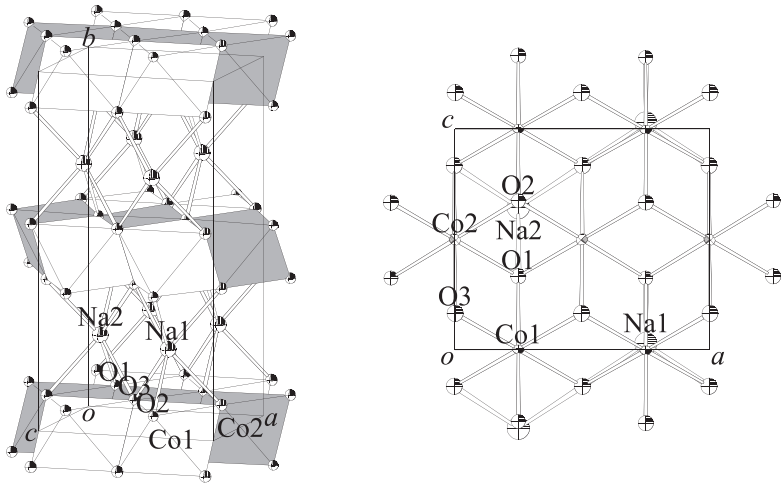

Figure 5. The crystal structures of $Na_{0.48}CoO_2$ at 297 K with the ellipsoids indicated at the 50% probability level: (a) the clinographic view with the white and shaded octahedra for Co1 and Co2, respectively, and (b) the projection on the *ac*-plane.

Table 9. Interatomic distances (Å) and Co valences for the superlattice structure of $Na_{0.48}CoO_2$ at 297 K, where the symmetry operations are: (*a*) $x,\ y,\ z$; (*b*) $x,\ y,\ -1+z$; (*c*) $\frac{1}{2}-x,\ y,\ z$; (*d*) $-x,\ -y,\ -z$; (*e*) $\frac{1}{2}+x,\ -y,\ -z$; (*f*) $-x,\ -y,\ 1-z$; (*g*) $x,\ -\frac{1}{2}-y,\ z$; (*h*) $x,\ y,\ 1+z$; (*i*) $\frac{1}{2}-x,\ y,\ 1+z$; (*j*) $x,\ -\frac{1}{2}-y,\ 1+z$; (*k*) $\frac{1}{2}-x,\ -\frac{1}{2}-y,\ 1+z$; (*l*) $x,\ \frac{1}{2}-y,\ z$; (*m*) $\frac{1}{2}+x,\ -y,\ 1-z$; (*n*) $-x,\ \frac{1}{2}+y,\ 1-z$; (*o*) $\frac{1}{2}+x,\ \frac{1}{2}+y,\ 1-z$; (*p*) $-x,\ -y,\ 2-z$; and (*q*) $1-x,\ -y,\ 2-z$.

Co–O		Na–O & metal–metal	
$Co1^a$–$O1^a$	1.86(2)	$Na1^a$–$O2^{a,g}$	2.346(16)
$Co1^a$–$O2^b$	1.87(2)	$Na1^a$–$O3^{h,i,j,k}$	2.469(11)
$Co1^a$–$O3^{a,c}$	1.903(11)	$Na2^a$–$O1^{a,l}$	2.363(18)
$Co1^a$–$O3^{d,e}$	1.887(11)	$Na2^a$–$O3^{f,m,n,o}$	2.475(11)
Co1 valence	3.64(4)	$Co1^a$–$Na1^b$	2.8287(16)
$Co2^a$–$O1^{a,f}$	1.895(11)	$Co1^a$–$Na2^b$	3.253(5)
$Co2^a$–$O2^{a,f}$	1.892(11)	$Co2^a$–$Na2^{a,f}$	3.198(2)
$Co2^a$–$O3^{a,f}$	1.90(2)	$Na1^a$–$Na2^{p,q}$	3.380(7)
Co2 valence	3.54(4)		

average structure (table 3). It is noted that the difference in the $Co1O_6$ and $Co2O_6$ coordinations leads to the relatively large anisotropic displacement parameters of Co for the average structure compared with those for other compositions (table 2). The Na1–O and Na2–O distances range from 2.346(16) to 2.475(11) Å, as expected from the value for six-coordinated Na ions [22].

3. Transport properties

The four-terminal electrical resistivity and thermoelectric power for all of the single-crystal specimens were measured using a dc method at temperatures from 4.2 to 300 K. The magnetization measurements for single crystals with $x \simeq 0.65$ were also performed at temperatures between 4.2 and 300 K using the Faraday method with a field of up to 1 T.

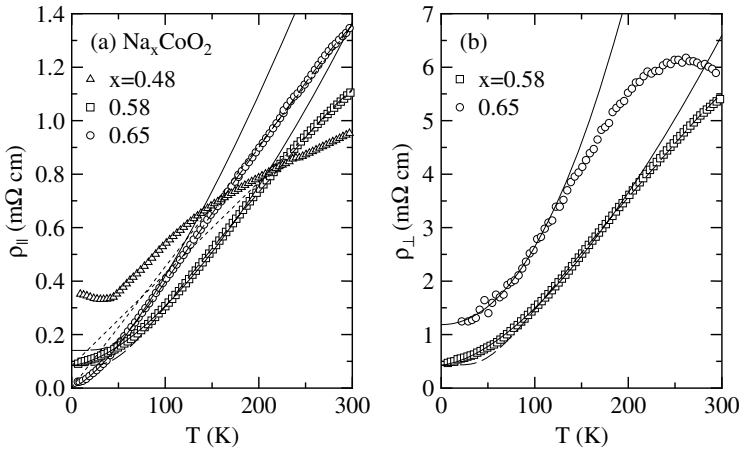

Figure 6. The temperature dependences of the electrical resistivities for (a) the direction parallel to the CoO_2 plane and (b) the normal direction of Na_xCoO_2 with $x \simeq 0.48$, 0.58 and 0.65. The full curves and the dotted lines denote fits to equation (4) with $p \simeq \frac{3}{2}$ and 1, respectively, and the dashed curves are based on the Bloch–Grüneisen model. Details of the parameters are described in the text.

The temperature dependences of the electrical resistivities for the direction parallel to the CoO_2 plane ($\rho_{\parallel}$) and for the normal direction ($\rho_{\perp}$) are shown in figures 6(a) and (b), respectively. No thermal hysteresis exists there. These results are significantly different from those for the polycrystalline specimens of Na_xCoO_2 with nominal composition $0.8 \leqslant x \leqslant 1$, where the low-temperature resistivities basically follow a dependence that is linear in temperature and exhibit anomalies at high temperatures [17]. Several important characteristics are revealed. For the composition with $x \simeq 0.58$, both $\rho_{\parallel}$ and $\rho_{\perp}$ are metallic for the temperature region measured. For $x \simeq 0.65$, $\rho_{\parallel}$ is metallic for all the temperature range and $\rho_{\perp}$ indicates a maximum at about 250 K. The ratio $\rho_{\perp}/\rho_{\parallel}$ for these compositions is about five at room temperature, so that the two-dimensionality for the transport is not so significant. The metallic temperature dependence of $\rho_{\parallel}$ for $x \simeq 0.48$ is weak compared with those for the above compositions, and exhibits a minimum at $T_c \simeq 50$ K, which indicates a transition to poor metallic states. The presence of T_c is similar to the previous result for $Na_{0.5}CoO_2$, which indicates nearly temperature-independent behaviour at $T > T_c$ [12]. Apparently, large residual resistivity for this composition may be attributed partly to the lattice imperfection and/or the inhomogeneous distribution of Na ions with the lowering of crystal symmetry caused by the soft-chemical treatment.

The temperature dependences of $\rho_{\parallel}$ and $\rho_{\perp}$ for $x \simeq 0.58$ below $T_{\rho} \simeq 200$ K are fitted with an equation

$$\rho = \rho_0 + AT^p, \tag{4}$$

where the first and second terms are the residual resistivity and the temperature-dependent formula related to the scattering mechanism. The full curves in figures 6(a) and (b) provide the following parameters: $\rho_0 = 83.8(7)$ $\mu\Omega$ cm and $A = 0.143(4)$ $\mu\Omega$ cm K^{-p} with $p = 1.595(5)$ for the direction parallel to the CoO_2 plane; and $\rho_0 = 427(3)$ $\mu\Omega$ cm and $A = 0.67(2)$ $\mu\Omega$ cm K^{-p} with $p = 1.597(5)$ for the normal direction. The self-consistent renormalization theory indicates that, near the critical boundary between the antiferromagnetic metal and normal metal, the resistivity at low temperatures shows a $T^{3/2}$ dependence [26]. Antiferromagnetic spin fluctuations have also been postulated from the neutron scattering

for $x = 0.75$ [27] and the muon spin rotation (μSR) for $x = 0.85$ [28], although these compositions are out of the present range. Thus, the temperature dependences for $x \simeq 0.58$ may be due to antiferromagnetic spin fluctuations. At $T > T_\rho$, $\rho_\parallel$ and $\rho_\perp$ deviate from the $T^{3/2}$ dependence and follow a T^1 dependence ($p = 1$ in equation (4)), as shown by the dotted line in figure 6(a). In this case, $A = 3.4339(4)$ $\mu\Omega$ cm K^{-1} with ρ_0 at the lower temperatures. This $T^{3/2} - T^1$ crossover around T_ρ may be understood qualitatively as a crossover between three dimensions and two dimensions in electronic states.

The $\rho_\parallel$ and $\rho_\perp$ data for $x \simeq 0.65$ can be discussed similarly. The fits to the data below $T_\rho \simeq 80$ K indicated by the full curves in figures 6(a) and (b) give the following parameters: $\rho_0 = 1.5(11)$ $\mu\Omega$ cm and $A = 0.69(3)$ $\mu\Omega$ cm K^{-p} with $p = 1.39(1)$ for the direction parallel to the CoO_2 plane; and $\rho_0 = 1.18(4)$ mΩ cm and $A = 0.09(10)$ $\mu\Omega$ cm K^{-p} with $p = 2.0(3)$ for the normal direction. The latter exponent, postulating Fermi liquid-like transport, is speculative, since the data are a little scattered. Thus, this composition also approximately exhibits the $T^{3/2}$ dependence, where T_ρ becomes lower compared with that for $x \simeq 0.58$. On the other hand, the dotted line obtained by a fit to the data above 150 K with $p = 1$ in equation (4) gives $A = 4.522(3)$ $\mu\Omega$ cm K^{-1}. The maximum phenomenon in $\rho_\perp$ is likely due to the renormalization effect of the Fermi surface by the fluctuations, as discussed previously for the transport properties of V_6O_{13} [29]. In addition, the temperature dependence of the magnetic susceptibility for this composition apparently follows a Curie–Weiss law with antiferromagnetic exchange coupling at all of temperatures measured. No long-range order exists.

Using the Bloch–Grüneisen formula instead of the second term in equation (4), the following parameters are obtained on the basis of the dashed curves in figures 6(a) and (b): for $x \simeq 0.58$, the Debye temperatures $\omega_D = 321.9(8)$ K for the CoO_2 plane and $\omega_D = 335.3(9)$ K for the normal direction; and for $x \simeq 0.65$, $\omega_D = 326(1)$ K for the CoO_2 plane. Here, the value of ρ_0 for $x \simeq 0.58$ is the same as that estimated above, but for $x \simeq 0.65$ it is 140(1) $\mu\Omega$ cm, which is two orders of magnitude larger than that described before. The Debye temperatures are within a normal range. The agreement between the data and this model is not bad above 50 K, but the deviation at lower temperatures is significant. Therefore, a simple electron–phonon scattering mechanism may be ineffective for this system.

The thermoelectric powers $S_\parallel$ for the direction parallel to the CoO_2 plane as a function of temperature are indicated in figure 7. All of the data are positive, indicating that the carriers are holes. For compositions with $x \simeq 0.58$ and 0.65, the thermoelectric powers are approximately linear in temperature, $S_\parallel \propto T$, as indicated by the full lines below $T_S \simeq 200$ and 80 K, respectively. These dependences do not appear for the polycrystalline specimens with nominal Na concentrations from 0.8 to 1, where thermally activated dependences seem to exist at low temperatures [17]. It should be noted that the above T_S values correspond to the $T^{3/2} - T^1$ crossover temperatures T_ρ for the resistivity. This suggests that, for temperatures smaller than the characteristic energy scale with antiferromagnetic spin fluctuations in three dimensions, the thermoelectric power is linear in temperature. Above T_S, the thermoelectric powers have values smaller than those expected from the T^1 dependence, but they still increase. The present result may be a touchstone for existing models for the large thermoelectric power in this system [30–32, 17].

The thermoelectric power for $x \simeq 0.48$ increases with positive power less than unity below 50 K, which corresponds to the metal–poor metal transition temperature T_c for the resistivity, while above T_c its temperature dependence is rather small and exhibits a slight hump (46 μV K^{-1}) at 120 K and a hollow (40 μV K^{-1}) at 220 K. Taking account of the weak dependence of the metallic resistivity above T_c, the nearly temperature-independent behaviour of thermoelectric power suggests that this composition is located near the metal–non-metal

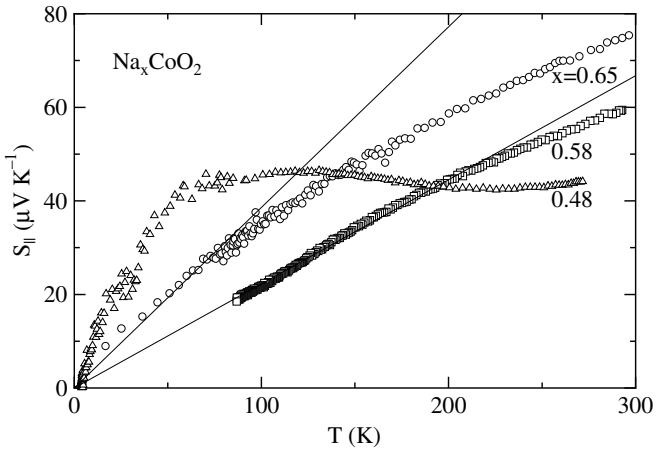

Figure 7. The temperature dependences of the thermoelectric powers for the direction parallel to the CoO_2 plane of Na_xCoO_2 with $x \simeq 0.48$, 0.58 and 0.65. The full lines indicate the dependence of $S_{\|} \propto T$.

boundary. This could be explained by the variable-range hopping (VRH) conduction having widely spread wavefunctions in two dimensions [33], which leads to a weak temperature dependence of resistivity, or non-Fermi-liquid behaviour in the low-dimensional Hubbard model [34]. On the other hand, below T_c the carrier localization becomes significant and the VRH conduction that follows $S \propto T^{1/3}$ and $T^{1/2}$ in two and three dimensions, respectively, is more effective.

4. Conclusions

The crystal structures of the triangular lattice system Na_xCoO_2 with compositions of $x \simeq 0.48$, 0.58 and 0.65 have been determined using x-ray four-circle diffraction. Here, the structural models of Na_xCoO_2 with x similar to the former two concentrations published previously are basically correct, but there exist non-obvious constraints for the refinement procedures. $Na_{0.58}CoO_2$ has an unmodulated $P6_3/mmc$-type structure with dimensions $a_h = 2.8180$ and $c_h = 11.005$ Å, while $Na_{0.65}CoO_2$ has a $P6_3/mmc$-type superlattice with $a_{sh} \simeq 2a_h$ and $c_{sh} \simeq c_h$, and $Na_{0.48}CoO_2$ indicates a $Pmmn$-type superlattice with $a_{so} \simeq 2a_h$, $b_{so} \simeq c_h$ and $c_{so} \simeq \sqrt{3}a_h$. The structural modulation for $x \simeq 0.65$ is attributed to the incomplete order of Na ions without any order for Co valence, while that for $x \simeq 0.48$ results in almost complete Na order and partial valence order for Co.

For $x \simeq 0.48$, the metal–poor metal transition takes place at $T_c \simeq 50$ K. This composition may be located near the metal–non-metal boundary, taking account of behaviours of the electrical resistivity and the thermoelectric power. Therefore, the structural modulation with the partial valence order described above might be related partly to a kind of charge density wave (CDW) accompanied by *imperfect* nesting of the Fermi surface in two dimensions, as is sometimes pointed out for the low-dimensionally conducting electron–phonon coupled system [35]. The electrical resistivities for $x \simeq 0.58$ and 0.65 follow a $T^{3/2}$ dependence below $T_\rho \simeq 200$ and 80 K, respectively, both for the direction parallel to the CoO_2 plane and for the normal direction, due to antiferromagnetic spin fluctuations in three dimensions. At higher temperatures, the resistivities for the CoO_2 plane indicate a T^1 dependence, which is likely attributed to an enhancement in two dimensionality. The thermoelectric powers also exhibit

different behaviours above and below T_ρ. For $x \simeq 0.65$, the resistivity maximum appears at about 250 K, which may be caused by the renormalization effect of the Fermi surface by the fluctuations.

As x increases, the temperature range where the transport is in two dimensions becomes wider. This tendency is consistent with the fact that the resistivities for the nominal composition of $0.8 \leqslant x \leqslant 1$ approximately follow the T^1 dependence for almost all of the temperatures measured. In addition, the dimensional crossover points for antiferromagnetic spin fluctuations reasonably link to the SDW-like transition temperature of about 20 K for $0.8 \leqslant x \leqslant 1$. This result indicates that the reduction in the interlayer distance with increasing Na concentration does not always weaken the two-dimensionality for electronic states of Na_xCoO_2.

A quantitative consistency between the crystal structures and the transport mechanisms revealed in this work should be tested from the theoretical viewpoint.

References

[1] Anderson P W 1973 *Mater. Res. Bull.* **8** 153
[2] Fazekas P and Anderson P W 1974 *Phil. Mag.* **30** 423
[3] See, for example, Farnell D J J, Bishop R F and Gernoth K A 2001 *Phys. Rev.* B **63** 220402
[4] Onoda M, Naka T and Nagasawa H 1991 *J. Phys. Soc. Japan* **60** 2550
[5] Bramwell S T and Harris M J 1998 *J. Phys.: Condens. Matter* **10** L215
[6] Takada K, Sakurai H, Takayama-Muromachi E, Izumi F, Dilanian R A and Sakaki T 2003 *Nature* **422** 53
[7] Terasaki I, Sasago Y and Uchinokura K 1997 *Phys. Rev.* B **56** R12685
[8] Fouassier C, Matejka G, Reau J-M and Hagenmuller P 1973 *J. Solid State Chem.* **6** 532
[9] Balsys R J and Davis R L 1996 *Solid State Ion.* **93** 279
[10] Jorgensen J D, Avdeev M, Hinks D G, Burley J C and Short S 2003 *Phys. Rev.* B **68** 214517
[11] Zandbergen H W, Foo M, Xu Q, Kumar V and Cava R J 2004 *Phys. Rev.* B **70** 024101
[12] Huang Q, Foo M L, Lynn J W, Zandbergen H W, Lawes G, Wang Y, Toby B H, Ramirez A P, Ong N P and Cava R J 2004 *J. Phys.: Condens. Matter* **16** 5803
[13] Foo M L, Wang Y, Watauchi S, Zandbergen H W, He T, Cava R J and Ong N P 2004 *Phys. Rev. Lett.* **92** 247001
[14] Yokoi M, Moyoshi T, Kobayashi Y, Soda M, Yasui Y, Sato M and Kakurai K 2005 *J. Phys. Soc. Japan* **74** 3046
[15] Sugiyama J, Brewer J H, Ansaldo E J, Hitti B, Mikami M, Mori Y and Sasaki T 2004 *Phys. Rev.* **69** 214423
[16] Wooldridge J, Paul D M K, Balakrishnan G and Lees M R 2005 *J. Phys.: Condens. Matter* **17** 707
[17] Ikeda T and Onoda M 2006 *J. Phys.: Condens. Matter* **18** 8673
[18] Sheldrick G M 1997 *SHELXS97* and *SHELXL97* University of Göttingen, Germany
[19] CrystalStructure *Crystal Structure Analysis Package* 2005 (The Woodlands, TX: Rigaku and Rigaku/MSC)
[20] Cromer D T and Waber J T 1974 *International Tables for X-Ray Crystallography* vol 4, ed J A Ibers and W C Hamilton (Birmingham: Kynoch) section 2
[21] Creagh D C and McAuley W J 1992 *International Tables for Crystallography* vol C, ed A J C Wilson (Boston, MA: Kluwer–Academic)
[22] Shannon R D 1976 *Acta Crystallogr.* A **32** 751
[23] Brese N E and O'Keeffe M 1991 *Acta Crystallogr.* B **47** 192
[24] Cooper R I, Gould R O, Parsons S and Watkin D J 2002 *J. Appl. Crystallogr.* **35** 168
[25] Farrugia L J 1999 *J. Appl. Crystallogr.* **32** 837
[26] Moriya T, Takahashi Y and Ueda K 1990 *J. Phys. Soc. Japan* **59** 2905 and references therein
[27] Helme L M, Boothroyd A T, Coldea R, Prabhakaran D, Tennant D A, Hiess A and Kulda J 2005 *Phys. Rev. Lett.* **94** 157206
[28] Bayrakci S P, Bernhard C, Chen D P, Keimer B, Kremer R K, Lemmens P, Lin C T, Niedermayer C and Strempfer J 2004 *Phys. Rev.* B **69** 100410(R)
[29] Onoda M, Ohki T and Uchida Y 2004 *J. Phys.: Condens. Matter* **16** 7863 and references therein
[30] Wang Y, Ronado N S, Cava R J and Ong N P 2003 *Nature* **423** 425
[31] Koshibae W and Maekawa S 2001 *Phys. Rev. Lett.* **87** 236603
[32] Takeuchi T, Kondo T, Takami T, Takahashi H, Ikuta H, Mizutani U, Soda K, Funahashi R, Shikano M, Mikami M, Tsuda S, Yokoya T, Shin S and Muro T 2004 *Phys. Rev.* B **69** 125410
[33] Brenig W, Döhler G H and Wölfle P 1973 *Z. Phys.* **258** 381
[34] See, for example, Stafford C A 1993 *Phys. Rev.* B **48** 8430
[35] See, for example, Onoda M, Fujishita H, Matsuda Y and Sato M 1987 *Synth. Met.* **19** 947